Improving the Performance of Sampled-Grating DBR Laser-Based Analog Optical Transmitters

Leif A. Johansson, *Member, IEEE*, Yuliya A. Akulova, Chris Coldren, and Larry A. Coldren, *Fellow, IEEE, Fellow, OSA*

***Abstract*—In this paper, the available analog link performance of integrated transmitters containing a sampled-grating distributed Bragg reflector laser, a semiconductor optical amplifier, and a modulator is evaluated. It is found that to provide a link gain and a low-noise figure, an RF preamplifier is required, and for this reason, spurious-free dynamic range (SFDR) including a preamplifier has been evaluated. An SFDR of 110-dBHz$^{2/3}$, a noise figure of 5.4 dB, and link gain of 6.9 dB at 5 GHz is obtained. It is further investigated how link SFDR can be improved by linearization techniques. Two novel approaches are proposed and demonstrated: first, predistortion by extraction of nonlinear components from an integrated second modulator exposed to the same wavelength, optical power and temperature for matched nonlinear terms; second, a novel linearized modulator configuration balancing electroabsorption and Mach–Zehnder modulation that can reach a null for both second- and third-order intermodulation products at a single bias point.**

***Index Terms*—Distributed Bragg grating lasers, electroabsorption, integrated optoelectronics, microwave photonics, optical communications, photonic integrated circuits.**

I. Introduction

INDIUM Phosphide (InP) integrated photonic circuits is an attractive technology for application in analog optical link applications. High-performance optical sources, modulators, and detectors are required to provide the necessarily high signal-to-noise ratio (SNR) needed for high dynamic range. The InP material system is sufficiently mature to offer these components while being compatible to low-cost production. Further, it is compatible with chipscale photonic integration of several components to form high functionality, compact transmitters, reducing overall component cost, and improving performance by cutting coupling losses between subcomponents. It has been shown how sampled-grating distributed Bragg reflector (SGDBR) lasers integrated with a semiconductor optical amplifier (SOA) and an electroabsorption modulator (EAM) forms a very attractive widely tunable optical transmitter for digital [1] and analog [2] optical link applications.

This paper builds on these previous results and summarizes recent efforts to improve the performance for analog link applications, in particular, efforts to improve link gain, noise, figure and dynamic range when applied in an analog optical link. Link gain in this paper is referred to link *power gain,* defined as the ratio of the detected RF power at the output of the link, to the link input RF power. Link noise figure is defined as the ratio of link output SNR to the input SNR, given thermal noise limit at the link input, the exact expression is $NF \equiv 10\log[N_{\mathrm{OUT}}/kTG]$, where N_{OUT} is output noise power, kT is input thermal noise power, and G is link power gain [3]. Spurious-free dynamic range (SFDR) here applies to the maximum achievable SNR in the optical link using a two-tone signal probe, with the restriction that the detected in-band intermodulation products remain lower or equal to the noise floor in a chosen noise bandwidth (typically normalized to 1-Hz noise bandwidth).

The paper is organized as follows. In Section II, a brief summary of baseline analog performance of SGDBR-based transmitters is given, with a particular emphasis on observed limitations to the performance, as it forms the base of the further efforts presented within this paper. This data has previously been published [2] and is here summarized as reference. Section III covers efforts to improve the noise performance of these transmitters. An improvement in link noise figure is observed by using a preamplifier. The performance at higher RF frequencies is also improved by employing optimized transmitter biasing schemes. The next two chapters are devoted to novel schemes to linearize the response of the modulator. A compensatory predistortion scheme is described in Section IV and a linearization technique employing a weak Mach–Zehnder (MZ) effect is described in Section V. The last section gives a summary of this work.

II. Baseline Performance

The reference device is described in detail in [1]. It consists of a SGDBR laser, an SOA, and an EAM, all integrated on the same InP chip using an offset quantum well structure to define active regions such as the laser gain section and SOA. The SG-DBR laser includes gain and phase sections positioned between two sampled grating distributed reflectors, sampled at different periods such that only one of their multiple reflection peaks can coincide at a time [4]. The overall wavelength coverage can be greater than 45 nm. The integrated SOA compensates for on-state modulator loss, and for cavity losses caused by free carrier absorption in the tuning sections, and allows wavelength independent power leveling. The EAM uses the same bulk quaternary waveguide as the tuning sections of the laser. The Franz–Keldysh effect in the bulk waveguide material provides for large spectral bandwidth and improved optical power handling capability.

The noise performance of the transmitter was limited by relative intensity noise at the RIN peak, improving with gain section injection current to at best -153 dB/Hz at 200-mA bias and room temperature. The added SOA noise could be observed in

Manuscript received November 20, 2006; revised July 20, 2007. This work was supported by the DARPA/MTO CS-WDM program.

L. A. Johansson and L. A. Coldren are with the Department of Electrical and Computer Engineering, University of California, Santa Barbara, CA 93106 USA (e-mail: leif@ece.ucsb.edu; coldren@ece.ucsb.edu).

Y. A. Akulova and C. Coldren are with the JDS Uniphase Corporation, Goleta, CA 93117 USA (e-mail: yuliya.akulova@jdsu.com; chris.coldren@jdsu.com).

Digital Object Identifier 10.1109/JLT.2007.916592

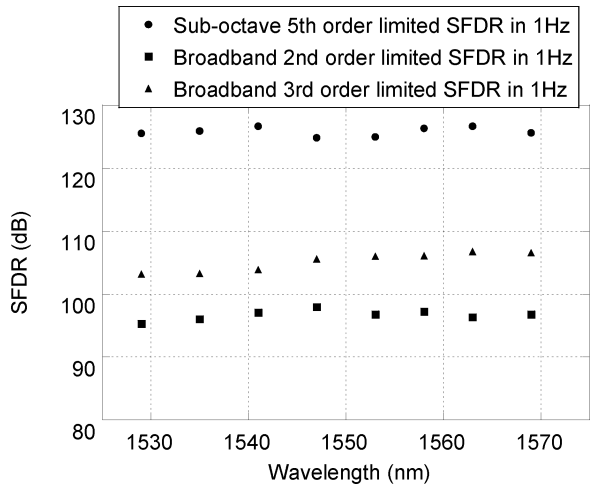

Fig. 1. Summary of measured EA SFDR when biased for broadband linear operation (minimum second-order intermodulation products) and biased for sub-octave linear operation (minimum third-order intermodulation products), normalized to 1-Hz noise bandwidth.

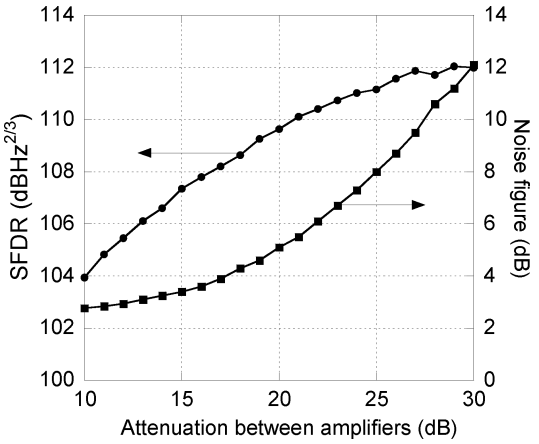

Fig. 2. Spurious-free dynamic range and link noise figure as a function of preamplification gain at 500-MHz modulation frequency.

the noise floor away from the RIN peak, typically below 2 GHz or at high frequencies.

A link gain of -20.7 dB was obtained when using the transmitter in an analog link. The gain can be increased by terminating the detector with a higher load [3]. However, since the link noise figure is not loss limited, but primarily limited by the relative intensity noise of the laser, this will not improve the noise figure of the link. In fact, the lowest noise figure of 32 dB was obtained in "low biased" condition, with lower link gain, but where the relative modulator slope sensitivity is greater. The potential for generating positive link gain was found to be severely limited by absorbed photocurrent in the modulator. In fact, the EA slope efficiency will asymptotically approach the limit given by one absorbed electron per photon, much like 100% quantum efficiency in a laser or a photodiode. This will make it challenging to reach positive loop gain (and low noise figure) when optical losses are present.

Like most optical modulators, the EAM has an inherently nonlinear response. Optimized linearity can be obtained by careful selection of the EA bias point, though. For broadband, second-order intermodulation limited operation, the optimum bias point is found around the highest absolute slope. The spurious-free dynamic range (SFDR, a common measure of analog link performance [3]) at 1552 nm was here 97 dB $\cdot$ Hz$^{1/2}$ second-order limited or 106 dB $\cdot$ Hz$^{2/3}$ third-order limited. A summary of the measured SFDR is found in Fig. 1. For sub-octave applications, where even-order intermodulation products can be filtered, the EA exhibits an optimum bias point where third-order intermodulation products in general can be cancelled out. The dynamic range is 126 dB $\cdot$ Hz$^{4/5}$, fifth-order limited, at this bias point and 1552 nm. It should be pointed out that the rapid growth of higher order intermodulation products with drive power still limits the available linear modulation depth, even at this bias point. Further, the SFDR was measured at 0.5 GHz, well below the RIN peak. With unoptimized laser bias, the SFDR can be degraded up to 10 dB at the peak RIN frequency.

III. Preamplified Link Performance

Obtaining a low noise figure in a simple optical link using this type of transmitter is currently not possible. Therefore, in most high-performance analog applications, the transmitter will be preceded by an electronic amplified to improve link gain and noise figure, and the transmitter performance in the presence of this amplifier must be considered.

As is well known, adding an amplifier in a microwave transmission system will in most cases degrade the dynamic range in the system [5]. This is also true here. Care must be taken in selecting preamplifiers such that the benefits in improved link gain and noise figure does not come at the cost of a greatly reduced dynamic range. This can be understood from the background of achieving a low noise figure. As the gain of the preamplifier is increased to reduce noise figure, the amplifier noise gradually starts to dominate the output noise floor with a resulting degradation in dynamic range. This is illustrated by the experimental data shown in Fig. 2. To obtain this data, two amplifiers were cascaded at the input of the transmitter. Both amplifiers have a gain of 29 dB, a noise figure of 2.4 dB and output IP3 of $+43.5$ dBm at 500 MHz. A 6-dB attenuator had to be placed between the last stage amplifier and the modulator in order to reduce RF reflections due to imperfect modulator matching. The overall preamplifier gain was then regulated by placing an adjustable RF attenuator between the two amplifiers. It can be observed that at high attenuation, the detected noise floor is predominantly RIN limited and the SFDR approaches the limit given by the combined nonlinearities of amplifiers and modulator, here at around 112 dB $\cdot$ Hz$^{2/3}$. As the preamplification gain is increased, the noise figure asymptotically approaches that of the first amplifier with an increasingly steep dynamic range penalty as the amplifier noise starts to dominate. In the following, an overall noise figure lower that 6 dB is targeted, to limit the dynamic range penalty.

In Fig. 2, the SFDR is third-order intermodulation limited, even in the sub-octave case. Without preamplification, the EAM can be biased such that third-order intermodulation products are cancelled out over a realistic bandwidth, given that some care is taken to produce an input two-tone probe signal free from distortion. In the preamplified case, the effect of cascaded nonlinearities and their cross-terms leads to a strong frequency

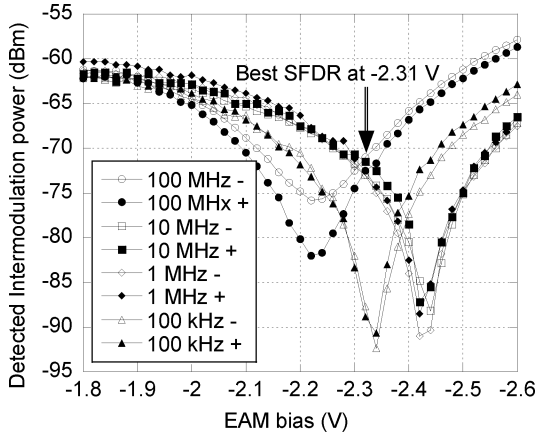

Fig. 3. Power of the third EAM order intermodulation products as a function of modulator bias for different RF frequency offset of a two-tone probe signal centered around 500 MHz.

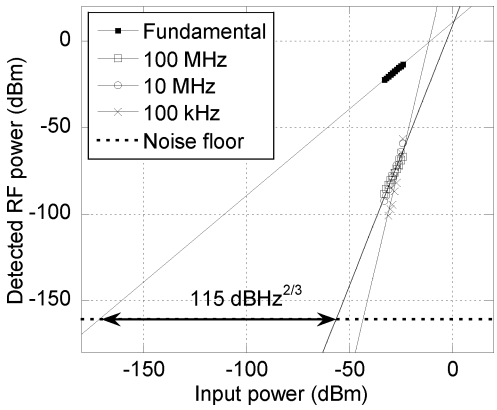

Fig. 4. Measured power of fundamental and third-order intermodulation terms and the corresponding SFDR around 500 MHz and for different separation between RF tones.

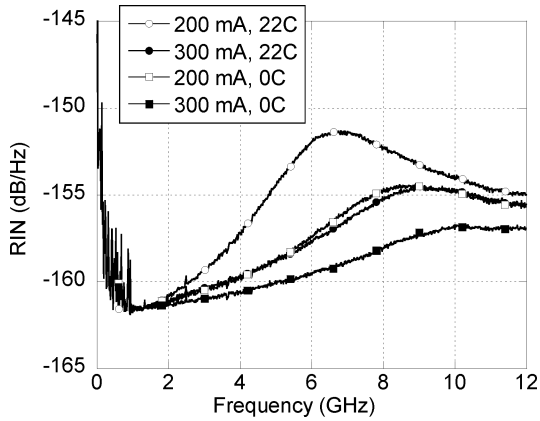

Fig. 5. Measured RIN at 200 and 300 mA and at 20 °C and 0 °C.

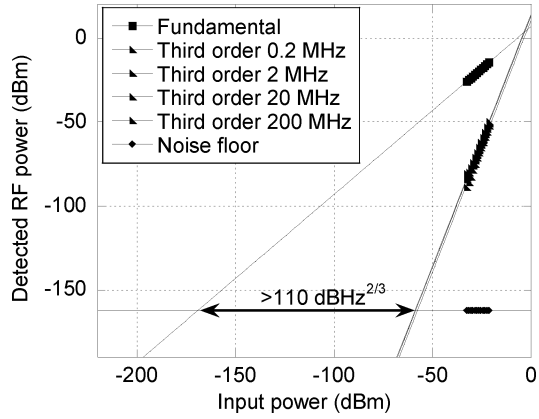

Fig. 6. Measured power of fundamental and third-order intermodulation terms and the corresponding SFDR around 5 GHz and for different separation between RF tones.

dependence on the bias point of minimum third-order distortion. Additional possible contributors to the wandering third-order minimum include internal effects in the optical transmitter, as frequency dependence at the difference frequency $\mathrm{f1}-\mathrm{f2}$, including thermal effects at small frequency separations. This is all illustrated by the results in Fig. 3, where the power of the third-order intermodulation products is recorded as a function of two-tone RF frequency offset from 500 MHz. We can observe that the minimum varies over a 0.2-V range. The sharp dips where fifth-order limited performance is obtained cannot be maintained over a realistic RF bandwidth, and the overall performance of the preamplified transmitter will effectively be best characterized by an SFDR with a third-order intermodulation limitation.

The resulting SFDR when biased at -2.31 V is shown in Fig. 4, where intermodulation terms are taken at a range of separation frequencies of a two-tone probe signal around 500 MHz. The resulting SFDR is 115 dB $\cdot$ Hz$^{2/3}$. To obtain this value, both gain section and SOA were biased at 200 mA at 18 °C at a wavelength of 1547 nm. The preamplifier gain was adjusted to balance the SFDR penalty and noise figure such that the overall link gain was $+10.5$ dB with a link noise figure of 5 dB for this result.

These results have all been taken at the moderate frequency of 500 MHz. At higher frequencies, above 2 GHz, the increased RIN has been shown to degrade the dynamic range of these transmitters [2]. To provide high performance over a wider frequency range, 5-GHz operation frequency is here targeted, the laser must be more aggressively biased. In accordance with previous observations [2], [6], the RIN peak is shifted to higher frequencies and increased damping of the RIN resonance is observed with increasing laser injection current. At room temperature and 200-mA injection current, the RIN was here measured at -154 dB/Hz at 5 GHz, as shown in Fig. 5. The measured low frequency noise can be controlled by using more quiet current drivers and improved decoupling to the tuning sections of the SGDBR laser. Increasing the injection current to 300 mA reduced the RIN level to -158 dB/Hz. Lowering the temperature from room temperature to 0 °C produced a similar improvement at 5 GHz from increased injection efficiency. Combining reduced temperature with higher injection current finally pushed the RIN down to -160 dB/Hz, sufficient to produce a respectable dynamic range even at this frequency.

A similar arrangement was built to produce a preamplified transmitter at 5 GHz as is used for the 500-MHz results presented above. A dual amplifier configuration with adjustable overall gain is used. The first amplifier has a noise figure of 2 dB and an IP3 of 30 dBm, and the second amplifier has a noise figure of 5 dB and an IP3 of 38 dBm. Again, a small attenuator (3 dB) was placed in-between the last stage amplifier and the modulator to control reflections. Fig. 6 shows the power of

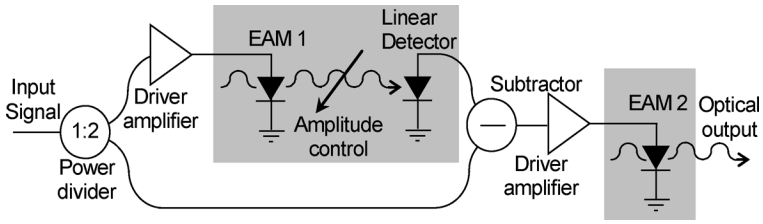

Fig. 7. Operational schematic of broadband linearization scheme. Shaded areas are integrated on the single InP chip shown in Fig. 8.

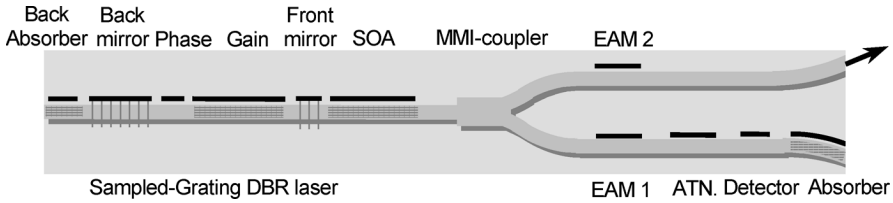

Fig. 8. Schematic of integrated photonic circuit.

the fundamentals and intermodulation terms at a range of separations of the two-tone probe. The preamplification gain was adjusted to produce a link noise figure of 5.4 dB and a link gain of 6.9 dB, resulting in an SFDR of 110 dB $\cdot$ Hz$^{2/3}$, limited by the nonlinearities of amplifiers and the modulator.

IV. Compensatory Predistortion

In the previous section, it was showed how the link gain and NF could be improved by adding preamplification. The high-performance frequency range was also extended by optimizing the drive conditions of the laser. However, no significant improvement in the dynamic range was generated in comparison to previous work [2].

Several linearization schemes can be considered to improve the linearity of these optical transmitters, not all are suitable for the particular requirements of a widely tunable transmitter that need to be compatible to a WDM environment. Perhaps the commercially most successful is using predistortion where improvements in performance can be achieved using an inexpensive and power efficient electronic circuit [7]. This approach can typically not adapt to changing operating conditions and requires that the response of the transmitter stays constant. It is, therefore, not suitable for integration with a widely tunable transmitter and a modulator that has wavelength-dependent response. An alternative is using feed-forward linearization where the modulated signal is tapped off and compared to the input to form a correcting signal to be added to the output [8]. In this way, any variations of the response are automatically corrected. However, the added signal must be separated in wavelength to avoid coherence effects, and is, therefore, not compatible to a WDM environment.

In the investigated approach, a predistortion circuit is constructed by measuring the nonlinearities of a first optical modulator to provide the predistorted input to a second modulator. This approach combines dynamic extraction of nonlinear response and WDM compatibility. Past demonstrations of this approach has typically been limited by the need to use two separate transmitters with slightly different response [9]. Here, the two modulators are integrated closely on a single chip, sharing a single optical source. Any variations in chip temperature, input power or wavelength now affect both modulators equally and can be dynamically compensated for.

Fig. 7 shows a schematic of the demonstrated predistortion arrangement. The input signal is split in a 2:1 ratio, where the lesser part is used to drive the predistortion link. The output of the link is then subtracted from the remainder of the input signal to form the predistorted input to the second transmitter. A driver amplifier and an optical attenuator are included in the link to ensure that the input power to the two transmitters stays equal for optimum distortion cancellation. In this demonstration, two discrete connectorized driver amplifiers are used. However, to fully take advantage of the linearization scheme, more integrated driver amplifiers should be used, preferably using two similar amplifiers sharing a common heat-sink.

Fig. 8 shows a schematic of the fabricated integrated photonic circuit. It is similar to the base device used previously with the difference that the power from the source is split into two EA modulators located in close proximity on the chip. The optical 3-dB bandwidth of this modulator is 8 GHz. A second reversed biased passive section acts as an optical attenuator and the detector then completes the on-chip optical link in one of the two waveguide paths. The second waveguide forms the optical output.

The SFDR of EAM2 in Fig. 8 without activating the predistortion path or using a driver amplifier is measured at 98 dBHz$^{2/3}$, when biased at maximum slope. This is about 7 dB lower than devices incorporating a single EA modulator [2], which can be attributed to the lower transmitted power of this particular prototype device. Connecting a driver amplifier to EAM2 with low power consumption (~ 800 mW) and low third-order intercept point ($+15$ dBm), the overall link gain is improved at the expense of a penalty in SFDR, now 93 dBHz$^{2/3}$. The left plot of Fig. 9 shows the captured RF spectrum around 500 MHz, where third-order intermodulation terms can be clearly observed.

Activating the on-chip predistortion link to compensate for nonlinearities, the third-order intermodulation terms can be reduced. The right plot of Fig. 9 shows the captured spectrum

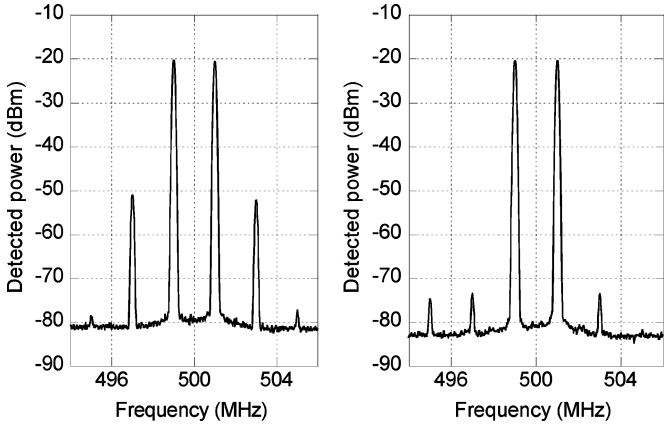

Fig. 9. RF spectra around 500 MHz for transmitter with and without predistortion.

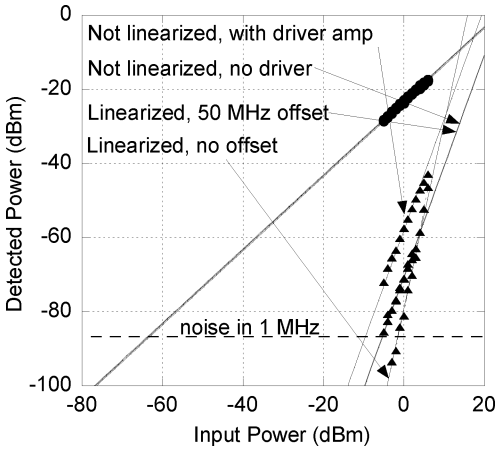

Fig. 10. SFDR of the predistorted transmitter with and without 50-MHz frequency offset from setting, and not predistorted with and without driver. The input power has been adjusted to facilitate comparison. The curves "Not linearized, no driver" and "Linearized, 50 MHz offset" overlap on this scale.

where the amplitude and phase response of the predistortion circuit has been matched. More than 20-dB suppression of third-order intermodulation terms is observed. This corresponds to a closely matched phase and amplitude in the summation of signal and predistortion link output. To generate 20 dB of intermodulation suppression, the power must be matched within 0.3 dB. A small penalty in higher order intermodulation terms is observed. This is a common effect in many linearization schemes and must be controlled so that it does not lead to a penalty. The measured SFDR at 500 MHz is compared to the uncompensated case in Fig. 10 where a fifth-order intermodulation-limited SFDR of 110 $\mathrm{dBHz}^{4/5}$ is obtained, more than compensating for the nonlinearities of the driver amplifier.

Like any linearization scheme that relies on gain matching, the effective bandwidth of the linearization is limited due to variations in frequency response. To investigate the effective bandwidth, the center frequency was shifted while keeping all adjustments in the predistortion part constant. The results are shown in Fig. 11, where the dynamic range is plotted as a function of frequency offset. A noise bandwidth of 1 MHz was chosen to take into account the varying slope of the intermodulation

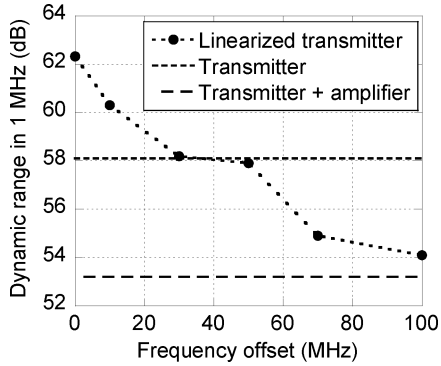

Fig. 11. Measured dynamic range in 1 MHz of the linearized transmitter as a function of shift in operating frequency.

terms with modulation power. It is observed that a 10-MHz frequency offset corresponds to only a 2-dB penalty in SFDR, while the added distortion of the driver amplifier is compensated for within a 50-MHz single-sided bandwidth. This fractional bandwidth can be improved by using more uniform response RF components or an equalizing circuit [10].

Even at zero frequency offset, the performance of the linearized transmitter does not reach the 115 $\mathrm{dBHz}^{2/3}$ measured in Fig. 4, using a single preamplified EAM. This is because of lower baseline performance of the optical and electrical devices, not an inherent limitation of the linearization technique. The 9-dB improvement in SFDR in 1-MHz bandwidth still represents a realistic number for the SFDR improvement practically achievable using careful amplitude and phase matching in this linearization scheme.

This linearization scheme has been shown to provide a limited amount of improvement in linearity in a compensatory manner. It is compatible with a widely tunable laser in that the generated predistorted signal is compensating for any wavelength dependence in the EA response. It has also been shown capable of compensating for amplifier nonlinearities, an important capability for application in realistic link applications, where the response of the amplifier also needs to be considered when low link noise figure is required. Here, this was limited by the use of discrete amplifier modules where the nonlinear terms not necessarily match. Ideally more closely integrated driver amplifiers with closely matched response should be used. One option is then to trade off the amplifier performance to reduce the power consumption of the transmitter, and compensating the loss of linearity. A highly linear amplifier can easily dominate the power budget of an analog transmitter. For automatic linearization over the entire tuning range, automatic predistortion gain control will need to be implemented to compensate for the variations in EA slope sensitivity with wavelength.

V. Linearized Modulator

The compensatory predistortion presented above is well suited to reach a high level of linearization over a narrow band or a moderate level of linearization over moderate band. The problem with this approach is gain imbalance due to very slight variations in the frequency response of the modulators. The cancellation then only takes place within this limited frequency

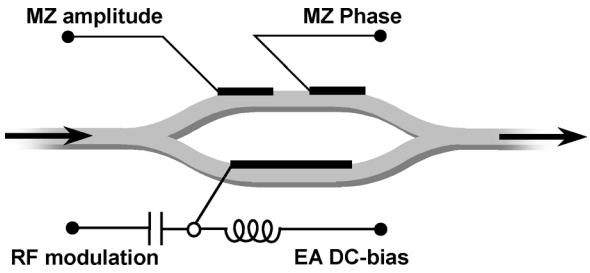

Fig. 12. Simple schematic of proposed modulator.

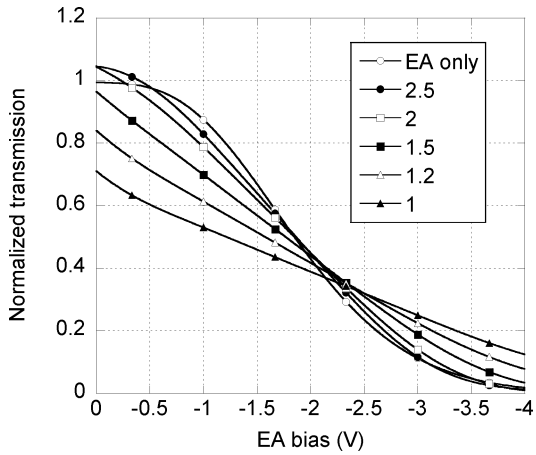

Fig. 13. Simulated linearized DC extinction curves for different ratios of equivalent EAM $V\pi$ to MZ $V\pi$.

range. We here propose and demonstrate a modulator structure that uses a single electrode to produce two modulation effects, which are then adjusted to produce an overall linearized response. Since only one electrode is being modulated, a linearized response over a wide frequency range can be expected.

The linearized modulator is based on a standard EAM. The EAM is inserted in a MZ configuration, where the other arm of the MZ is not being modulated. This produces a composite response which is given by the combination between electroabsorption and interference within the MZ modulator structure given by the electrorefraction in the modulator. Fig. 12 shows a simple schematic of the proposed modulator. The electroabsorption is modeled after the response of a Franz–Keldysh modulator, where both phase and amplitude is modulated. The total response of the modulator is then a combination of EA and MZ modulation. The EA modulator is biased at maximum slope sensitivity with minimum second-order intermodulation products. The phase control of the MZ is regulated to the corresponding operating point, with minimized second-order intermodulation but at opposite slope. A linearized response is then generated by regulating the amplitude balance between the two arms, such that third-order intermodulation products of the EA and MZ are cancelled out.

Fig. 13 shows a sample of simulated linearized responses for different ratio between the equivalent $V\pi$ of the EAM and MZ $V\pi$. For a high ratio, the power of third-order intermodulation products generated by the MZ is large relative to those produced by the EAM. In this case, a highly unbalanced MZ is required for third-order intermodulation cancellation. As the $V\pi$ ratio decreases, the voltage range where a constant slope is obtained increases as the cancellation of higher order intermodulation terms also improves. Reducing the $V\pi$ ratio even more, a penalty in overall slope sensitivity appears, as the absolute slope of the MZ becomes comparable to that of the EAM. A $V\pi$ ratio of 2 represents a good operating point with low penalty in slope sensitivity, and still a wide voltage range with constant slope.

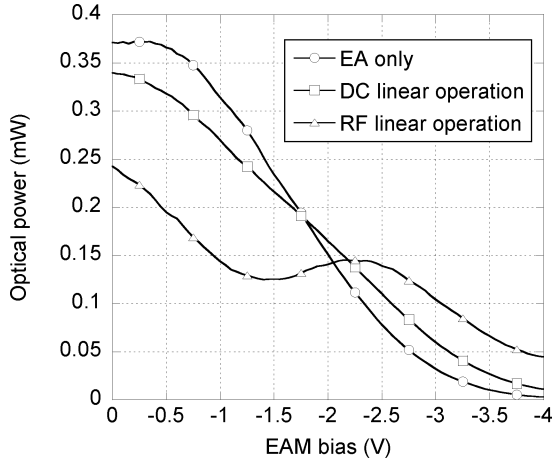

Fig. 14. Measured modulator DC extinction curves using the EAM only, and for the bias points (MZ phase + MZ balance) for a linearized DC transfer function and the transfer function where linearized RF modulation is observed.

Further, in addition to simultaneous cancellation of second and third-order intermodulation, the model shows that careful adjustment of the three DC controls would allow additional cancellation of fourth-order intermodulation products. In practice below, this operating point was never reached.

The device used to experimentally verify the proposed linearized modulator configuration is similar to that described in [11]. It consists of a widely tunable sampled grating DBR laser, a semiconductor amplifier (SOA) and a MZ modulator, all integrated on the same InP chip. The modulator consists of multimode interference (MMI) sections and 600-μm-long lumped electrodes. The laser-modulator uses a common waveguide structure, where passive sections, such as used in the MZ modulator, is defined by selective removal of an offset active quantum-well material. The bulk material of the electrodes of the MZ exhibit both electrorefraction and electroabsorption at reverse applied bias. This makes the MZ a suitable candidate for demonstration of the above linearization scheme, which requires both effects. MZ amplitude control is then achieved when reverse bias is applied to the second MZ electrode, absorbing part of the light. Amplitude independent phase control is obtained in a separate phase control section, using carrier injection phase tuning.

Fig. 14 shows the DC extinction at 1542-nm wavelength. The extinction of EA only is obtained when the second electrode of the MZ is deeply reverse biased (< -6 V) for full absorption. With the correct balance between EA and MZ effects, an overall linearized response at DC is obtained, shown in Fig. 14. This operating point is not the same as for linear operation at RF modulation. The response at DC is affected by slow thermal effects that do not affect the response at RF mod-

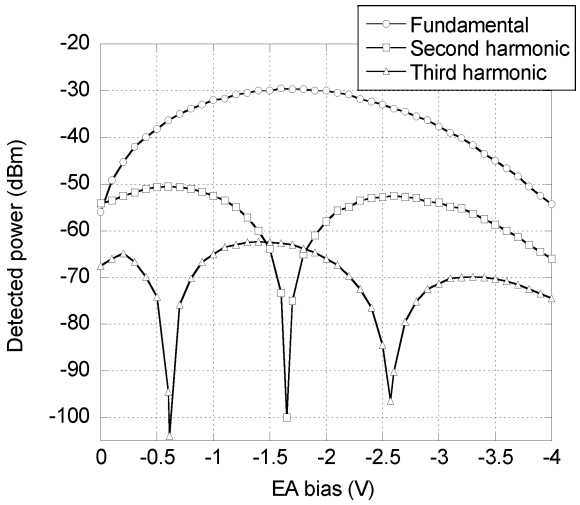

Fig. 15. Detected power of fundamental and intermodulation products using EA modulation only for 4-dBm modulation power per tone and at 1542 nm.

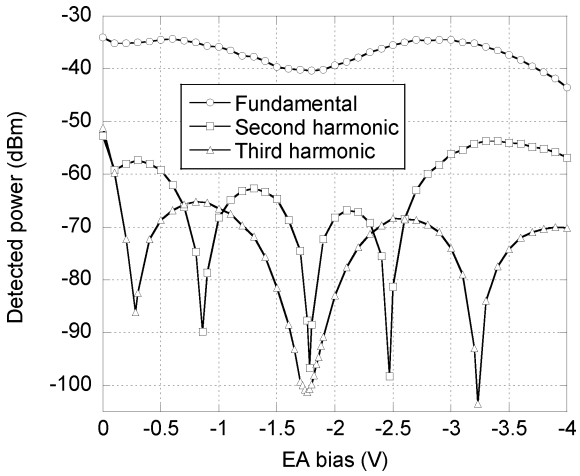

Fig. 16. Detected power of fundamental and intermodulation products using the linearized modulator for 4-dBm modulation power per tone and at 1542 nm.

ulation around a constant DC bias point. The DC response obtained at the linear bias point for RF, shown in Fig. 14, indicates that the electrorefractive effect is relatively more affected by slow heating, with a higher effective $V\pi$ at RF than is indicated by DC data. Currently, the SOA bias current was reduced to limit MZ input optical power so that the I–V product of each MZ electrode remained less than 100 mW at -6 V, I being the absorbed photocurrent. The reduced optical power also limited the total link gain and available SFDR. The spurious-free dynamic range (SFDR) was evaluated using two-tone modulation at f1, f2 $= 500 \pm 10$ MHz. Odd-order intermodulation products were measured either at either $2\text{f1} - \text{f2}$ or $2\text{f2} - \text{f1}$, whichever term was the greatest. Even-order intermodulation products were measured at $\text{f1} + \text{f2}$.

Figs. 15 and 16 shows a comparison between EA only and the linearized modulator of the power of fundamental and intermodulation products as a function of applied electrode bias. Using EA modulation only, a characteristic behavior for most modulators is observed, where at maximum slope, second-order

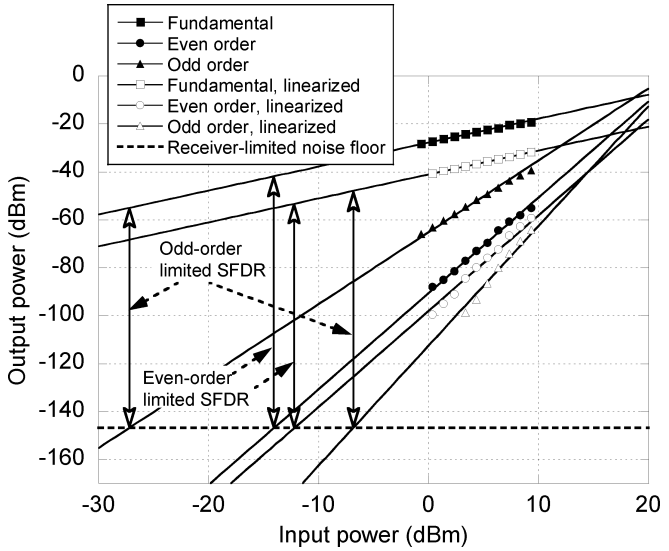

Fig. 17. Measured SFDR, limited by even or odd-order intermodulation products for the EAM and for the linearized modulator at 1542 nm and for receiver limited noise floor.

intermodulation products are minimized, while third-order intermodulation products are prevalent. For the linearized modulator, local minima for both odd and even order products are obtained at the same bias voltage, -1.67 V. This represents the central advantage of this type of linearized modulator, the ability to linearize the response for broadband application. Due to slow thermal effects, the power of the fundamental does not stay constant over a wide DC voltage range, as would be expected form a linearized behavior. Instead, a local minimum with a slight curvature is found around the linear bias point.

The measured SFDR is shown in Fig. 17 for both EAM and the linearized modulator. For the EAM, second-order intermodulation was cancelled at maximum slope. The SFDR, as limited by odd and even order products was 91.9 dB $\cdot$ Hz$^{2/3}$ and 104.9 dB $\cdot$ Hz$^{3/4}$, respectively. For the linearized modulator, both second and third-order intermodulation products could be cancelled, and odd-order limited SFDR increased to 98.9 dB $\cdot$ Hz$^{4/5}$. Even-order limited SFDR was reduced to 93.4 dB $\cdot$ Hz$^{3/4}$. The main reason for reduction is lower slope sensitivity of the linearized modulator. The noise floor was in all cases limited by receiver noise.

Linearized modulation was obtainable over the entire tuning range of the integrated SGDBR laser. To investigate the dependence on emission wavelength, the laser was tuned to the extremes of the tuning range and the SFDR was measured. The results are summarized in Table I. The linearization can reduce the relative power of third-order intermodulation products to a higher degree than second-order intermodulation, as the EA was biased for minimum second-order intermodulation to start with. However, the modulation sensitivity was reduced by more than 10 dB over the tuning range, resulting in a very modest improvement in SFDR. The cause of this is the nonoptimized balance between the relative effect of MZ and EA modulation. Potentially, with the right modulator material parameters, there could be a very low penalty in overall slope sensitivity, resulting in a broadband enhancement in odd-order limited SFDR by greater

TABLE I
SFDR LIMITED BY ODD (2f1 − f2) OR EVEN (f1 + f2) ORDER INTERMODULATION PRODUCTS FOR LINEARIZED AND NOT LINEARIZED EAM AT DIFFERENT WAVELENGTHS

Wavelength	EA-modulator		Linearized EA-modulator	
	SFDR (2f1-f2)	SFDR (f1+f2)	SFDR (2f1-f2)	SFDR (f1+f2)
1520.9 nm	89.9 dB·Hz$^{2/3}$	103.5 dB·Hz$^{3/4}$	97.8 dB·Hz$^{4/5}$	92.7 dB·Hz$^{3/4}$
1542.0 nm	91.9 dB·Hz$^{2/3}$	104.9 dB·Hz$^{3/4}$	98.9 dB·Hz$^{4/5}$	93.4 dB·Hz$^{3/4}$
1574.4 nm	91.7 dB·Hz$^{2/3}$	104.5 dB·Hz$^{3/4}$	99.3 dB·Hz$^{4/5}$	92.2 dB·Hz$^{3/4}$

than 10 dB with no penalty in even-order limited SFDR. However, unless overall slope sensitivity is sacrificed, a high-chirp EA must be developed that corresponds to a highly efficient MZ effect.

VI. CONCLUSION

In this paper, we have performed further investigations in transmitters formed by the integration of a widely tunable SGDBR laser with an SOA and modulator for analog optical link applications. It has been shown that by adding a preamplifier to the transmitter, low noise figure and optical link gain can be achieved. It is also shown that in a practical link application, with preamplification, a fifth-order dependence of intermodulation terms will practically not be reached, as a strong dependence of linear bias point to frequency separation using a two-tone probe signal is observed. The preamplified sub-octave SFDR was 115 dBHz$^{2/3}$ (5 dB-NF and 10.5-dB link gain) at 500 MHz and 110 dBHz$^{2/3}$ (5.4 dB-NF and 6.9-dB link gain) at 5 GHz, using a low-RIN operating point.

Improved dynamic range can be achieved using any of a number of linearization schemes. Two novel approaches have been investigated in this work. The first uses an compensatory predistortion scheme where an integrated second modulator is used to extract nonlinear terms. 20-dB suppression of intermodulation terms has been demonstrated. This approach will respond to any changes in modulator response due to wavelength, temperature and other factors. It has also been shown to be capable of providing linearization of preamplifiers, allowing the use of more nonlinear but efficient amplifiers. The main drawback of this approach is the requirement for gain matching over the operating frequency range, making this approach most attractive for narrowband applications.

The second linearization approach investigated is a linearized modulator fashioned from a combination of electroabsorption and MZ modulation that can null both third and second-order intermodulation products at a single bias point. This approach has the potential for wideband linearization, being a single electrode approach with no requirement for gain matching. The limitation is here the requirement for triple bias control; EA bias, MZ phase, and MZ balance. These must be further adjusted for any changes in modulator response due to input wavelength, temperature, etc.

REFERENCES

[1] L. A. Johansson, J. T. Getty, Y. A. Akulova, G. A. Fish, and L. A. Coldren, "Sampled Grating DBR laser-based analog optical transmitters," *J. Lightw. Technol.*, vol. 21, no. 12, pp. 2968–2976, Dec. 2003.

[2] Y. A. Akulova, G. A. Fish, P. C. Koh, C. Schow, P. Kozodoy, A. Dahl, S. Nakagawa, M. Larson, M. Mack, T. Strand, C. Coldren, E. Hegblom, S. Penniman, T. Wipiejewski, and L. A. Coldren, "Widely-tunable electroabsorption-modulated sampled grating DBR laser transmitter," *IEEE J. Sel. Topics Quant. Electron.*, vol. 8, no. 6, pp. 1349–1357, Nov./Dec. 2002.

[3] E. I. Ackerman and C. H. Cox, "RF fiber-optic link performance," *IEEE Microw. Mag.*, vol. 2, no. 4, pp. 50–58, Dec. 2001.

[4] V. Jayaraman, Z.-M. Chuang, and L. A. Coldren, "Theory, design, and performance of extended tuning range semiconductor laser with sampled grating," *IEEE J. Quant. Electron.*, vol. 29, no. 6, pp. 1824–1834, Jun. 1993.

[5] C. H. Cox, *Analog Optical Links: Theory and Practice*. Cambridge, U.K.: Cambridge Univ. Press, 2004, ch. 3.

[6] H. Shi, D. Cohen, J. Barton, M. Majewski, L. A. Coldren, M. C. Larson, and G. A. Fish, "Relative intensity noise measurements of a widely tunable sampled-grating DBR laser," *IEEE Photon. Technol. Lett.*, vol. 14, no. 6, pp. 759–761, Jun. 2002.

[7] G. C. Wilson, T. H. Wood, M. Gans, J. L. Zyskind, J. W. Sulhoff, J. E. Johnson, T. Tanbun-Ek, and P. A. Morton, "Predistortion of electroabsorption modulators for analog CATV systems at 1.55 μm," *J. Lightw. Technol.*, vol. 15, pp. 1654–1662, Sep. 1997.

[8] T. Ismail, C. P. Liu, J. E. Mitchell, and A. J. Seeds, "Interchannel distortion suppression for broadband wireless over fibre transmission using feed-forward linearised DFB laser," in *Proc. IEEE Int. Topical Meeting Microwave Photonics*, Oct. 4–6, 2004, pp. 229–232.

[9] J. Yu, T. Y. Chang, G. C. Wilson, T. H. Wood, N. J. Sauer, J. E. Johnson, T. Tanbun-Ek, and P. A. Morton, "Linearization of 1.55-μm electroabsorption modulated laser bydistortion emulation and reversal for 77-channel CATV transmission," *IEEE Photon. Technol. Lett.*, vol. 10, no. 3, pp. 433–435, Mar. 1998.

[10] R. Sadhwani, J. Basak, and B. Jalali, "Adaptive electronic linearization of fiber optic links," in *Proc. Optical Fiber Communications Conf.*, Mar. 2003, vol. 2, pp. 477–479.

[11] Y. A. Akulova, G. A. Fish, P. Koh, P. Kozodoy, M. Larson, C. Schow, E. Hall, M. Marchand, P. Abraham, and L. A. Coldren, "10 Gb/s Mach–Zehnder modulator integrated with widely-tunable sampled-grating DBR laser," presented at the Optical Fiber Communication Conf., Washington, DC, 2004, TuE4, on CD-ROM.

Leif A. Johansson (M'04) received the Ph.D. degree in engineering from University College London, London, U.K., in 2002.

He is currently a Research Scientist at the University of California, Santa Barbara. His current research interests include design and characterization of integrated photonic devices for analog and digital applications and analog photonic systems and subsystems.

Yuliya A. Akulova, photograph and biography not available at the time of publication.

Chris Coldren, photograph and biography not available at the time of publication.

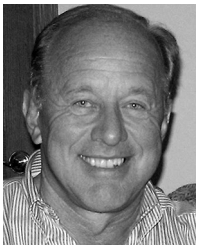

Larry A. Coldren (S'67–M'72–SM'77–F'82) received the Ph.D. degree in electrical engineering from Stanford University, Stanford, CA, in 1972.

He is the Fred Kavli Professor of Optoelectronics and Sensors at the University of California, Santa Barbara (UCSB). HeAfter 13 years in the research area at Bell Laboratories, he joined UCSB in 1984, where he now holds appointments in Materials and Electrical and Computer Engineering and is the Director of the Optoelectronics Technology Center. In 1990, he co-founded Optical Concepts, later acquired as Gore Photonics, to develop novel VCSEL technology, and, in 1998, he co-founded Agility Communications, recently acquired by JDS Uniphase Corporation (JDSU), Goleta CA, to develop widely tunable integrated transmitters. At Bell Labs, he initially worked on waveguided surface-acoustic-wave signal processing devices and coupled-resonator filters. He later developed tunable coupled-cavity lasers using novel reactive-ion etching (RIE) technology that he created for the then new InP-based materials. At UCSB, he continued work on multiple-section tunable lasers, inventing the widely tunable multielement mirror concept in 1988, which is now used in some JDSU products. During the late 1980s, he also developed efficient vertical-cavity multiple-quantum-well modulators, which led to novel vertical-cavity surface-emitting laser (VCSEL) designs that provided unparalleled levels of performance. He continues to be active in developing new photonic integrated circuit (PIC) and VCSEL technology, including the underlying materials growth and fabrication techniques. In recent years, for example, he has been involved in the creation of efficient all-epitaxial InP-based and high-modulation speed GaAs-based VCSELs, as well as a variety of InP-based PICs incorporating numerous optical elements for widely tunable integrated transmitters, receivers, and wavelength converters operating up to 40 Gb/s. He has authored or coauthored over 800 papers, five book chapters, one textbook, and has been issued 61 patents.

Prof. Coldren has presented dozens of invited and plenary talks at major conferences. He is a Fellow of OSA and IEE, a member of the National Academy of Engineering, and the recipient of the 2004 John Tyndall Award.